

Research paper

Investigation and modelling approach of the mechanical properties of compacts made with binary mixtures of pharmaceutical excipients

V. Busignies ^a, B. Leclerc ^a, P. Porion ^b, P. Evesque ^c, G. Couarraze ^a, P. Tchoreloff ^{a,*}^a Centre d'études Pharmaceutiques de l'Université Paris XI, Châtenay-Malabry, France^b Université d'Orléans, Orléans, France^c Ecole centrale de Paris, Châtenay-Malabry, France

Received 24 January 2006; accepted in revised form 16 March 2006

Available online 5 June 2006

Abstract

Three pharmaceutical excipients (microcrystalline cellulose, lactose, anhydrous calcium phosphate) and their binary mixtures were compacted to form compacts of various mean porosities. Some mechanical properties (Young's modulus, tensile strength and Brinell hardness) were studied on these compacts. The mechanical properties of the binary mixtures were not proportional to the mixture composition expressed in mass. More, for all the properties, a negative deviation was always observed from this linear relationship. In reference to a composition percolation phenomenon, critical mass fractions were detected from the graph mechanical property vs. mass composition of a mixture. The results obtained with Brinell hardness differed from the results of the Young's modulus and the tensile strength, i.e. the most plastic material in the binary mixture controlled the mixture behaviour. Secondly, a predictive model based on a statistical approach was proposed for the Young's modulus and the tensile strength. The validity of this model was verified on experimental data, and an interaction parameter used to characterize the affinity of the two compounds was calculated. Finally, the X-ray tomography technique was applied to the compacts of cellulose/phosphate mixtures to obtain cross-sections images of the compacts. The analysis of the cross-sections images allowed explaining the no linear relationship of the different mechanical properties results observed on these binary mixtures.

© 2006 Elsevier B.V. All rights reserved.

Keywords: Binary mixtures; Compactibility; Tensile strength; Young's modulus; Brinell hardness; Modelling; X-ray tomography; Percolation

1. Introduction

Tablets produced in pharmaceutical industry are generally made with a number of components. However, the study of the properties of compacted mixtures has received little attention. Data of single materials are generally available and the right formulation is generally obtained after lots of trials. Whereas, it must be useful to predict the tablet properties from the data obtained with the mixture com-

ponents. Numerous workers have investigated the compaction of binary mixtures [1–8]. In most cases, no simple relationship is found from the compaction properties of the single materials and their proportions in the mixture, and the mechanical properties of tablets compressed from binary mixtures are in general not linearly related to the properties of tablets obtained from single materials. Many studies show three possibilities for this relationship, a positive/negative effect or a linear relationship [8]. These results are attributed to the degree of magnitude of the bonds between particles of different materials. In that case, the aim of all studies of tableting powder mixtures will be to use the known properties of single materials in order to predict the compaction behaviour of mixtures. Due to the variety and the complexity of tableting properties, there

* Corresponding author. IFR-141, "Innovation thérapeutique: du Fondamental au Médicament", Centre d'études Pharmaceutiques de l'Université Paris XI, 5 rue Jean-Baptiste Clément, 92296 Châtenay-Malabry, France. Tel.: +33 1 46 83 56 11; fax: +33 1 46 83 58 82.

E-mail address: pierre.tchoreloff@cep.u-psud.fr (P. Tchoreloff).

Nomenclature

V:	microcrystalline cellulose, Vivapur 12 [®]	D:	indenter diameter
F:	partly amorphous lactose, Fast Flo [®]	D:	diameter of the indentation imprint
A:	anhydrous calcium phosphate, A TAB [®]	n:	number of experimental trials used in the calculus of the average values
VA:	Vivapur 12 [®] /TAB [®] mixtures	Y_{AA}, Y_{BB} :	properties of the single materials (A and B) in the 1st approach of the statistical model
VF:	Vivapur 12 [®] /Fast Flo [®] mixtures	Y_{AB} :	property resulting from the binary interaction {AB} in the 1st approach of the statistical model
AF:	A TAB [®] /Fast Flo [®] mixtures	Y_{ww} :	interaction parameter in 1st approach of the statistical model
ε :	mean compact porosity	Y_{AAA}, Y_{BBB} :	properties of the single materials (A and B) in the 2nd approach of the statistical model
P_y :	mean yield pressure	Y_{ABB}, Y_{BAA} :	properties resulting from the triplet interaction {ABB} and {BAA} in the 2nd approach of the statistical model
σ_c :	compaction pressure	Y_{ww1}, Y_{ww2} :	interaction parameters in 2nd approach of the statistical model
σ_r :	tensile strength	x and $(1-x)$:	mass proportions of the two components of a binary mixture in the statistical model (Section 3.3)
E :	Young's modulus		
H_b :	Brinell hardness		
F_m :	maximal load applied in microindentation and Young's modulus measurement		
F_r :	maximal load applied in tensile strength measurement		
p :	distance between the two support of the three point single beam test		
δ :	central deflexion in the three point single beam test		
h and l :	thickness and width of the parallelepipedical compacts		

are few studies in the literature which propose a model for mechanical properties of compacted mixtures [9,10]. A satisfactory theory enabling the prediction of the mixture properties does not exist at present. Recently, the percolation theory was used to explain the change of properties of compacted binary mixtures [11,12]. In the case of powder mixtures, it is a composition percolation phenomenon and the important parameter is the phase fractions. Binary mixtures of powders can be considered as systems made of three phases: two particles phases and pore space. According to a composition percolation phenomenon and at a constant porosity, the mixture can be in three situations [12–14]. If an A/B mixture is considered, when the fraction of B is small, these particles are isolated inclusions and form a dispersed phase. The component in a greater proportion (A) and/or with the smaller particle size forms a continuous phase. The presence of a dispersed phase changes the behaviour of the continuous phase due to the localization of tensions. When the fraction of B increases, the particles of B form aggregates. At last, when the fraction of B particles is high, a percolating B particle network appears for a B concentration corresponding to the percolation threshold, p_{c1} . The phase A ceases to exist as an infinite cluster for a B concentration corresponding to the upper percolation threshold, p_{c2} . Between the two thresholds, the two components form two interpenetrating percolating networks. To know in which situation the mixture is could be helpful to understand the behaviour of powder mixtures. More, in binary mixture containing particles of

both components A and B, three kinds of interactions may occur [15]: (1) A bonds preferentially with A and B bonds preferentially with B, (2) the affinity of A (B) for A (B) is the same as the affinity of A for B, (3) A bonds preferentially with B. Thus, the percolation thresholds in a compact of a binary mixture depend on the relative concentrations and the relative bond-forming properties [14].

The present work was performed to analyse the compaction behaviour of single materials (microcrystalline cellulose, lactose and anhydrous calcium phosphate) and their binary mixtures. This analysis was based on the measurement of some mechanical properties like Young's modulus, tensile strength and Brinell hardness. The three pharmaceutical excipients were chosen because of their different compaction behaviour [16,17]. The single materials and the binary mixtures were compacted and their mechanical properties were studied. First, the variations of these properties with the mixture composition are presented. Secondly, the objective of this study is to define the behaviour and to propose a model for the tensile strength and the Young's modulus of compacted binary mixtures using the mechanical properties obtained with the single excipients. X-ray microtomography technique was also performed with one of the binary mixtures to obtain cross-sections images of the compacts. These images were analysed to characterize and study the heterogeneity in the compacts. It was also correlated to the different mechanical properties observed.

2. Materials and methods

2.1. Excipients

Granular fractions (between 100 and 180 μm) of pharmaceutical excipients were used: a microcrystalline cellulose (Vivapur 12[®], 5601210932, JRS, Germany, kindly given by JRS), a partly amorphous lactose (Fast Flo[®], 8500042062, Foremost, US) and an anhydrous calcium phosphate (A TAB[®], GW930187, Rhodia, France). The mean particle sizes in volume were obtained by laser diffraction (Coulter LS 230) in conditions of validity of Fraunhofer's theory (162 $\mu\text{m} \pm 35 \mu\text{m}$ for A TAB[®], 134 $\mu\text{m} \pm 36 \mu\text{m}$ for Fast Flo[®] and 152 $\mu\text{m} \pm 48 \mu\text{m}$ for Vivapur 12[®]). These excipients consolidate by different mechanisms and are characterized by their mean yield pressure (P_y) which is deduced from the Heckel's plots [18,19]. Vivapur 12[®] (V) consolidates by plastic deformation ($P_y = 54 \text{ MPa} \pm 4 \text{ MPa}$) and A TAB[®] (A) by fragmentation ($P_y = 530 \text{ MPa} \pm 5 \text{ MPa}$). Fast Flo[®] (F) has an intermediate behaviour ($P_y = 111 \pm 2 \text{ MPa}$) [16,17]. Before use, the fractions were stored in a closed chamber at $48\% \pm 6\%$ of relative humidity for at least three days. The apparent particle density of each fraction was determined using an helium pycnometer (Acupyc 1330[®], Micromeritics, USA), see Table 1.

2.2. Preparation of binary mixtures

The binary mixtures (Vivapur 12[®]/A TAB[®]: VA, Vivapur 12[®]/Fast Flo[®]: VF and A TAB[®]/Fast Flo[®]: AF) were prepared in mass percentages (20/80, 35/65, 50/50, 65/35, 80/20 w/w) with a Turbula mixer (type T2C, Willy A Bachofen, Switzerland) at 50 rpm for 5 min (the degree of filling of a 550 ml vessel is about

50%). The mixtures were labelled with their mass composition. For example, VA36 means a mixture of Vivapur 12[®]/A TAB[®] with a respective concentration of 35% and 65% in mass (see Table 1). The apparent particle densities of the binary mixtures were calculated from the values of the mixture components according to their weight proportions in the mixture [20] (Table 1):

$$\frac{100}{d_{\text{part mix}}} = \frac{X_1}{d_{\text{part1}}} + \frac{X_2}{d_{\text{part2}}}, \quad (1)$$

where, d_{part1} , d_{part2} and $d_{\text{part mix}}$ are the apparent particle densities of the single components and their mixtures, respectively, X_1 and X_2 are the weight fractions of the constituent powders.

2.3. Formation of compacts

A mass suitable to obtain zero porosity at a theoretical compact thickness of 5 mm (about 1.8 g for F and V, about 3.3 g for A) was used to obtain parallelepipedical compacts ($40 \times 6 \text{ mm}^2$) of single-component powders and binary mixture powders using an instrumented hydraulic press (Perrier Labotest[®], France) [21] at compaction pressures ranging (σ_c) from 4 to 210 MPa. After compaction, the compacts were stored for at least three days in a closed chamber at a relative humidity of $48\% \pm 6\%$. In order to calculate the mean compact porosity, ε , the compacts were measured (micrometer Digimatic 293[®], Mitutoyo, Japan, with a resolution of 1 mm) and exactly weighted (Sartorius BP 2215[®], Germany, with a resolution of 0.1 mg) after total elastic recovery.

$$\varepsilon = 1 - \frac{\text{apparent density}}{\text{apparent particle density}}. \quad (2)$$

Table 1

Apparent particle densities for the single-component powders (experimental values, $n = 3$) and the binary mixtures powders (calculated values using Eq. (1))

Notation	Powder	Apparent particle density (g cm^{-3})
VIV	Vivapur 12 [®]	1.5402 ± 0.0005
AT	A TAB [®]	2.8103 ± 0.0002
FF	Fast Flo [®]	1.5309 ± 0.0001
VF82	80% Vivapur 12 [®] + 20% Fast Flo [®] (w/w)	1.5383
VF63	65% Vivapur 12 [®] + 35% Fast Flo [®] (w/w)	1.5369
VF55	50% Vivapur 12 [®] + 50% Fast Flo [®] (w/w)	1.5355
VF36	35% Vivapur 12 [®] + 65% Fast Flo [®] (w/w)	1.5341
VF28	20% Vivapur 12 [®] + 80% Fast Flo [®] (w/w)	1.5328
VA82	80% Vivapur 12 [®] + 20% A TAB [®] (w/w)	1.6932
VA63	65% Vivapur 12 [®] + 35% A TAB [®] (w/w)	1.8296
VA55	50% Vivapur 12 [®] + 50% A TAB [®] (w/w)	1.9898
VA36	35% Vivapur 12 [®] + 65% A TAB [®] (w/w)	2.1808
VA28	20% Vivapur 12 [®] + 80% A TAB [®] (w/w)	2.4124
AF82	80% A TAB [®] + 20% Fast Flo [®] (w/w)	2.4078
AF63	65% A TAB [®] + 35% Fast Flo [®] (w/w)	2.1743
AF55	50% A TAB [®] + 50% Fast Flo [®] (w/w)	1.9821
AF36	35% A TAB [®] + 65% Fast Flo [®] (w/w)	1.8211
AF28	20% A TAB [®] + 80% Fast Flo [®] (w/w)	1.6842

2.4. Measurement of mechanical properties

Mechanical properties were studied on parallelepipedical compacts after total elastic recovery using a micropress prototype [22]. The experimental procedure and the evaluation of the mechanical properties were described in detail in previous work [23]. The experimental parameters specific to this study are shown in Table 2.

The Young's modulus (E) and the tensile strength (σ_r) were obtained using a three point single beam test. The parallelepipedical compacts were stressed using a 2 mm flat punch at a constant velocity of $0.050 \text{ mm min}^{-1}$. To only measure the elastic response of the compact, a series of loading/unloading cycles were applied (Table 2). The Young's modulus (E in GPa) was obtained from the slope of the loading part of the last cycle. The maximum loading (F) corresponds to about 80% of the load that causes compact fracture (F_r)

$$E = \frac{F_m \cdot p^3}{4 \cdot \delta \cdot h^3 \cdot l}, \quad (3)$$

where F is the load applied, p is the distance between the two supports (34.12 mm), δ is the central deflexion and h , l are the thickness and the width of the compact, respectively.

Secondly, F_r was measured and used to calculate the tensile strength (σ_r in MPa) using the following equation:

$$\sigma_r = \frac{3 \cdot F_r \cdot p}{2 \cdot l \cdot h^2}, \quad (4)$$

where p is the distance between the two supports (i.e. 34.12 mm) and h , l are the thickness and the width of the compact, respectively.

The Brinell hardness (H_b in MPa) was obtained using a microindentation test [23]. A stress was applied on the top side of the parallelepipedical compact by a spherical indenter with a 2.38 mm diameter at a rate of 0.06 mm min^{-1} . The maximal displacement of the indenter and the relaxation time were adjusted to the sample composition (Table 2). The Brinell hardness H_b was calculated by the following equation [24]:

$$H_b = \frac{2 \cdot F_m}{(\pi \pi \cdot D) \cdot (D - \sqrt{D^2 - d^2})}, \quad (5)$$

where F is the maximal load applied, D is the indenter diameter and d is the diameter of the indentation surface.

Table 2

Specific parameters for the study of the mechanical properties (All the other parameters are those of the reference [23])

	Young's modulus, E	Brinell hardness, H_b
Vivapur 12 [®]	5 loading/unloading cycles	Indenter displacement: 0.1 mm Relaxation time: 5 min
Fast Flo [®]	3 loading/unloading cycles	Indenter displacement: 0.08 mm Relaxation time: 3 min
A TAB [®]	3 loading/unloading cycles	Indenter displacement: 0.06 mm Relaxation time: 1 min

For each mechanical property and each pressure target, three tablets were tested. But, it was not possible to obtain these tablets under exactly the same compaction pressure (i.e. with the same porosity) and to provide mean and standard deviations for the experimental results.

2.5. Mechanical properties versus porosity relationship

The mechanical properties of a compact were plotted versus the porosity ε and fitted by the following empiric relationship [25,26]:

$$A = A_0 \cdot e^{-b \cdot \varepsilon}, \quad (6)$$

where A is one of the mechanical properties previously described (E , σ_r , H_b), ε is the mean compact porosity, A_0 is the mechanical property at $\varepsilon = 0$ and b is a parameter deduced from the fitting of the experimental curve.

Due to the range of porosities observed with the compacts containing A TAB[®] (Table 3), the mechanical properties of VA and AF compacts (interpolated values obtained with the exponential relationship) were compared using a 35% porosity value. For VF compacts, porosities of 20% and 35% were used.

2.6. X-ray microtomography measurement

The X-ray microfocus computed tomography (X-ray μ CT) method is a nondestructive inspection technique which provides cross-sectional images in different planes from the sample [27]. The principle of the third generation CT imaging is illustrated in Fig. 1. The sample is placed on a precision turntable in a divergent beam of X-rays. A detector (which is in fact a one-dimension or a two-dimension array of detectors) is used to measure the local intensity distribution of a diverging X-ray beam transmitted through the sample, as the sample is rotated step by step angle in the beam. The sample position from the X-ray source determines the geometrical magnification (i.e. the resolution which is also limited by the detector size) according to the principle of the cone-beam geometry. This leads to a series of radiographs also called projection images at different viewing angles. From this set, one can reconstruct a three-dimensional representation of the structure and/or a composition distribution within a sample, using a mathematical algorithm based on the Beer–Lambert law of absorption (see Eq.

Table 3

Range of mean porosities obtained with the parallelepipedical compacts of the three single excipients

	Compact porosity, ε (%)	
	$\sigma_c = 4 \text{ MPa}$	$\sigma_c = 210 \text{ MPa}$
A TAB [®]	57	35
Fast Flo [®]	52	11
Vivapur 12 [®]	63	10

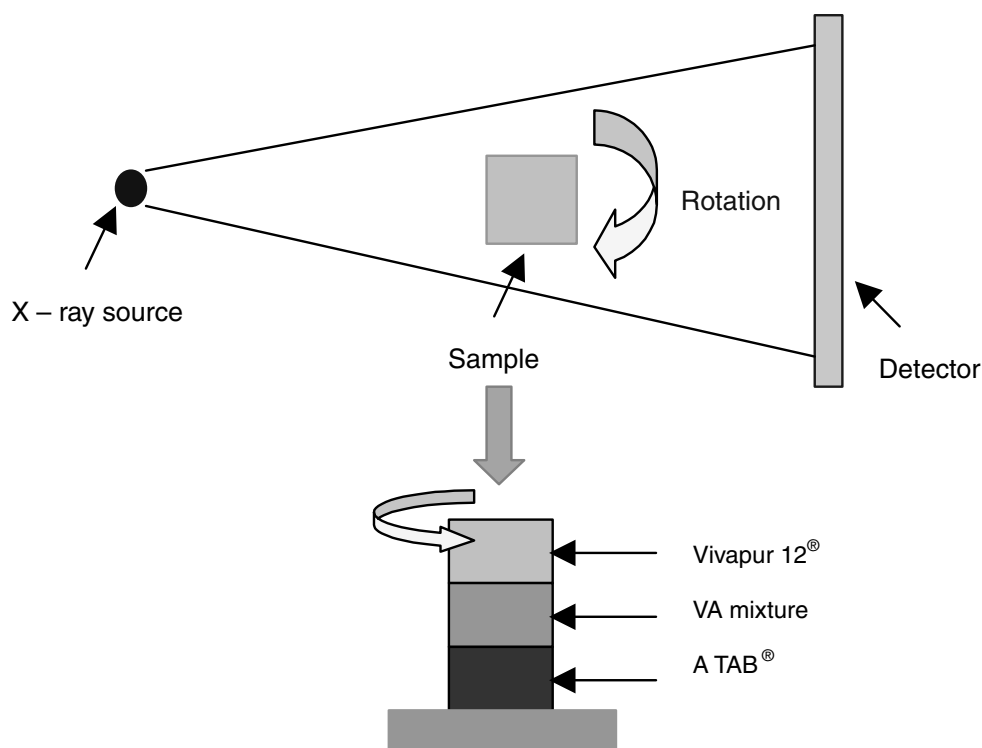


Fig. 1. X-ray microtomography measurement in the case of the compacted Vivapur 12®/A TAB® mixtures.

7). This reconstruction is called a tomogram; it has a spatial volume resolution, which is called a voxel. The tomogram can be decomposed in a series of cross-sectional images in a chosen plane, and these cuts can be interpreted in terms of density or composition distribution after the calibration process.

According to the Beer–Lambert law, the dependence of the intensity $I(x)$ of the X-ray beam after its crossing through a layer of homogeneous material of thickness x is related to the initial intensity I_0 and the linear X-ray attenuation coefficient of the material μ (it is a characteristic material coefficient) through [28]:

$$I(x) = I_0 \cdot e^{-\mu \cdot x}. \quad (7)$$

X-ray micro-CT images were provided for a cubic sample (about $5 \times 5 \text{ mm}^2$) of parallelepipedical compacts of VA mixtures obtained at 120 MPa. A Skyscan-1072 High-resolution desk-top micro-CT system (SkyScan, Aartselaar, Belgium) was used. The principle of the technique in the case of this study is illustrated in Fig. 1. The technique and its application to pharmaceutical compacts were described in more detail in references [16,17,29]. In this work, the scanning parameters were as follows: the X-ray source was operated at a voltage U of 67 kV and a current I of 90 μA (i.e. $P = 6 \text{ W}$) with an exposure time of 3.472 s per projection and an angular increment of 0.23° . The resolution size in the three directions after image reconstruction was $14.20 \mu\text{m}$ for VA36 and VA28 mixtures and $12.02 \mu\text{m}$ for the other VA samples. All the cross-sectional images obtained with this technique were analysed using the ImageJ software [30].

3. Results and discussion

3.1. Mechanical properties of the single materials

3.1.1. Young's modulus, E

Fig. 2 shows the variation of the Young's modulus with the mean porosity in the case of the parallelepipedical compacts of the single excipients. For porosities larger than 35%, A is the hardest of the three excipients, since for this range of porosity, its Young's modulus is the largest ($E_{35\%A} = 3.33 \text{ GPa}$ whereas $E_{35\%F} = 0.96 \text{ GPa}$ and $E_{35\%V} = 0.59 \text{ GPa}$). For all the porosities, the Young's modulus values of V show that it is more prone to the

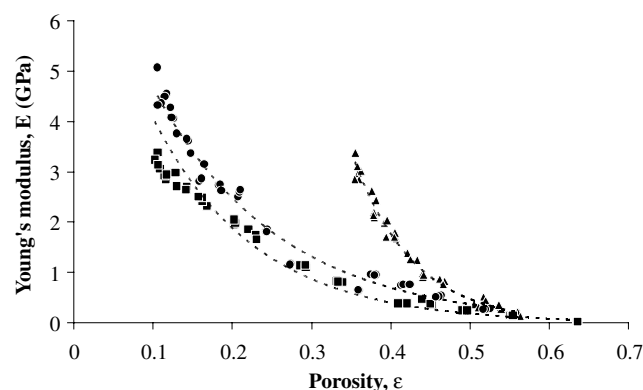


Fig. 2. Relationship between Young's modulus (E) and the mean porosity (ϵ) for the compacts composed of the single materials. Key: \blacktriangle , A TAB® ($E = 339.97e^{-13.16\epsilon}$, $R^2 = 0.9772$); \bullet , Fast Flo® ($E = 8.81e^{-6.34\epsilon}$, $R^2 = 0.9737$); \blacksquare , Vivapur 12® ($E = 8.81e^{-7.71\epsilon}$, $R^2 = 0.9592$).

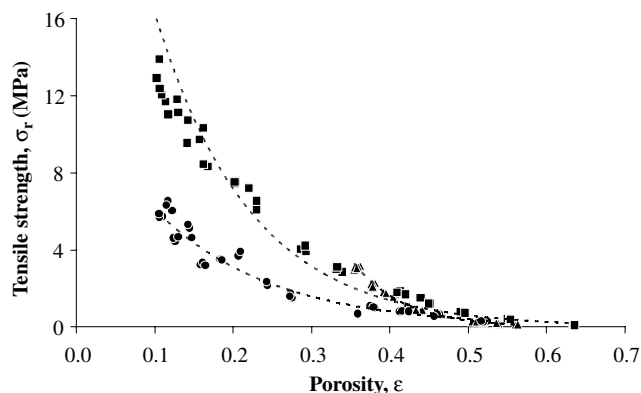


Fig. 3. Relationship between the tensile strength (σ_t) and the mean porosity (ε) for the compacts composed of the single materials. Key: \blacktriangle , A TAB[®] ($\sigma_t = 852.8e^{-15.66\varepsilon}$, $R^2 = 0.9950$); \bullet , Fast Flo[®] ($\sigma_t = 12.0e^{-6.74\varepsilon}$, $R^2 = 0.9714$); \blacksquare , Vivapur 12[®] ($\sigma_t = 37.1e^{-8.22\varepsilon}$, $R^2 = 0.9611$).

deformation. For example, at a porosity of 20%, the Young's modulus of V is 1.88 GPa and that of F is 2.48 GPa.

3.1.2. Tensile strength, σ_t

The plot of the tensile strength of the compacted three excipients versus the mean porosity is given in Fig. 3. For compact porosities larger than 35%, the tensile strength of A compacts ($\sigma_{t35\%A} = 3.55$ MPa) is larger than three times those of F ($\sigma_{t35\%F} = 1.13$ MPa) and higher than one and half those of V ($\sigma_{t35\%V} = 2.09$ MPa). For compact porosities smaller than 35%, the tensile strength observed with V compacts is also larger than those of F compacts.

3.1.3. Brinell hardness, H_b

The Brinell hardness is a characteristic of the surface elastoplasticity of a compact. Contrary to the Young's modulus and the tensile strength which characterize the sample volume, the Brinell hardness is a property of the sample surface. The change of Brinell hardness with the

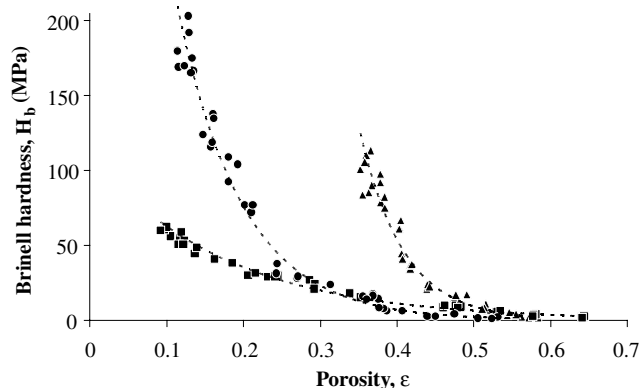


Fig. 4. Relationship between Brinell hardness (H_b) and the mean porosity (ε) for the compacts composed of the single materials. Key: \blacktriangle , A TAB[®] ($H_b = 62607e^{-17.6\varepsilon}$, $R^2 = 0.9768$); \bullet , Fast Flo[®] ($H_b = 811.3e^{-11.9\varepsilon}$, $R^2 = 0.9755$); \blacksquare , Vivapur 12[®] ($H_b = 111.3e^{-5.7\varepsilon}$, $R^2 = 0.9787$).

mean compact porosity is plotted in Fig. 4. In the range of porosity covered by the compact of A, the surfaces of A compacts have a higher Brinell hardness than those of the two other excipients. The hardness of V and F compacts is in the same order for these porosities. When the compact porosity becomes lower than 35%, the Brinell hardness of F compacts becomes higher than the hardness of V compacts. The hardness of V compacts shows the lowest increase when the porosity decreases.

3.2. Mechanical properties of the binary mixtures

3.2.1. Young's modulus, E

The Young's moduli of the mixtures are compared at a constant mean porosity $\varepsilon = 35\%$ (and also $\varepsilon = 20\%$ in the case of VF mixtures) and for various mixture compositions expressed in mass (Fig. 5). Indeed, for all the mixtures, the variation of the Young's modulus with the mixture composition cannot be described by a simple linear mixing rule, since a large negative deviation from this relationship is observed.

VF mixtures (diamond-shaped symbols in Fig. 5). It can be noted that the Young's modulus of a mixture can be smaller than the one of the two single materials. This is observed at $\varepsilon = 35\%$ and 20% with VF mixtures. Furthermore, the Young's modulus is nearly at a constant level between 20% and 80% in mass of F. With reference to the composition percolation theory, these two particular values may be closed to the percolation thresholds of the two materials (these two particular values are also called critical mass fractions).

VA mixtures (circle symbols in Fig. 5). A is harder than V since its Young's modulus is about seven times the one of V for a porosity of 35%. A constant value is observed when concentrations of A are less than 60% w/w. This value is about the one of V. Then, for these mixture compositions, it is thought that the V particles form a "soft" percolated skeleton which controls the total elastic behaviour. Beyond a threshold of 65–70% w/w of A in the mixture, A starts dominating the system and the Young's modulus increases. Therefore, introducing little proportions of A in a network of V does not affect the rigidity of the compact. It is only much above 70% w/w of A (which corresponds to the percolation threshold of V) that the material becomes harder. So, the percolation threshold for A cannot be detected.

AF mixtures (triangular symbols in Fig. 5). At $\varepsilon = 35\%$, the Young's modulus decreases when F is introduced in the AF mixtures until a minimum is observed for a F concentration of 50% w/w, for which the Young's modulus is smaller than the F modulus itself. Then, E increases at larger proportions of F (50–80% w/w). At 80% w/w of F, E reaches the value of the Young's modulus of F and remains constant likely from 80% to 100% w/w.

3.2.2. Tensile strength, σ_t

The tensile strengths of the mixtures are evaluated at a constant porosity of $\varepsilon = 35\%$ (and also $\varepsilon = 20\%$ in the case

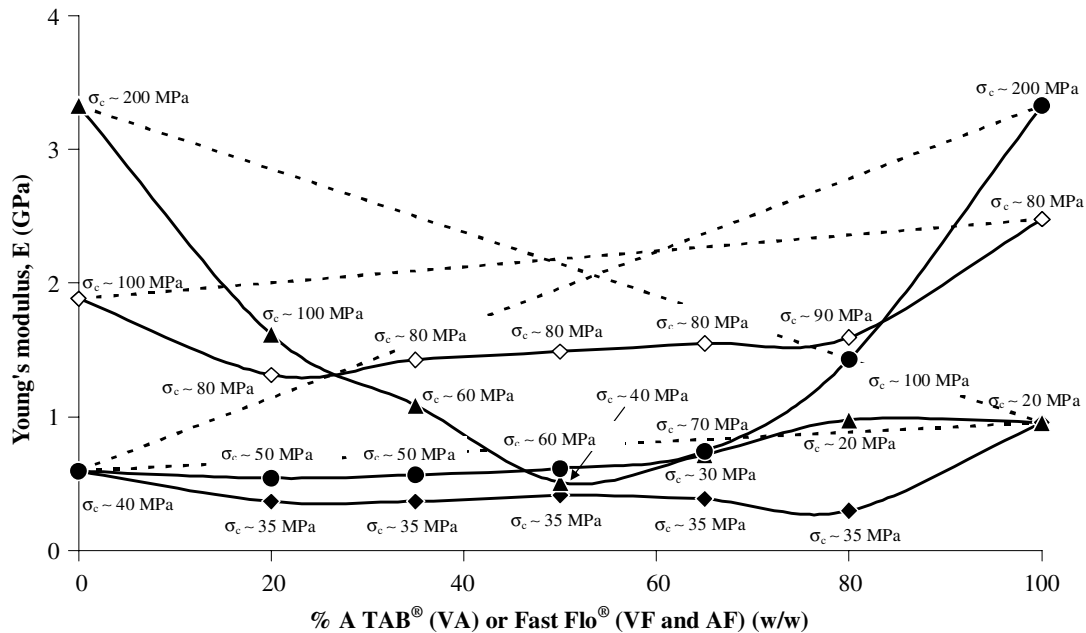


Fig. 5. Young's modulus (E , interpolated values) as a function of binary mixture composition (w/w) for compact mean porosities (ε). The dotted line represents the result of the use of a linear simple mixing rule. σ_c is the compaction pressure applied to obtain the corresponding E values. Key: ●, VA (with $\varepsilon = 35\%$); ◇ and ◆, VF (with $\varepsilon = 20\%$ and 35%); ▲, AF (with $\varepsilon = 35\%$).

of VF mixtures) and their variations versus the mixture composition are shown in Fig. 6. Like for the Young's modulus, the variation of the tensile strength with the mixture composition is not described by a simple linear mixing rule, and a negative deviation from this rule is observed. Also, there are three different trends for the three mixtures,

similar to what is observed in the case of the Young's modulus.

VF mixtures (diamond-shaped symbols in Fig. 6). The tensile strength deviates significantly from the linear rule in the whole studied range. Between critical mass concentrations of about 20% and 80% of F, the tensile strength

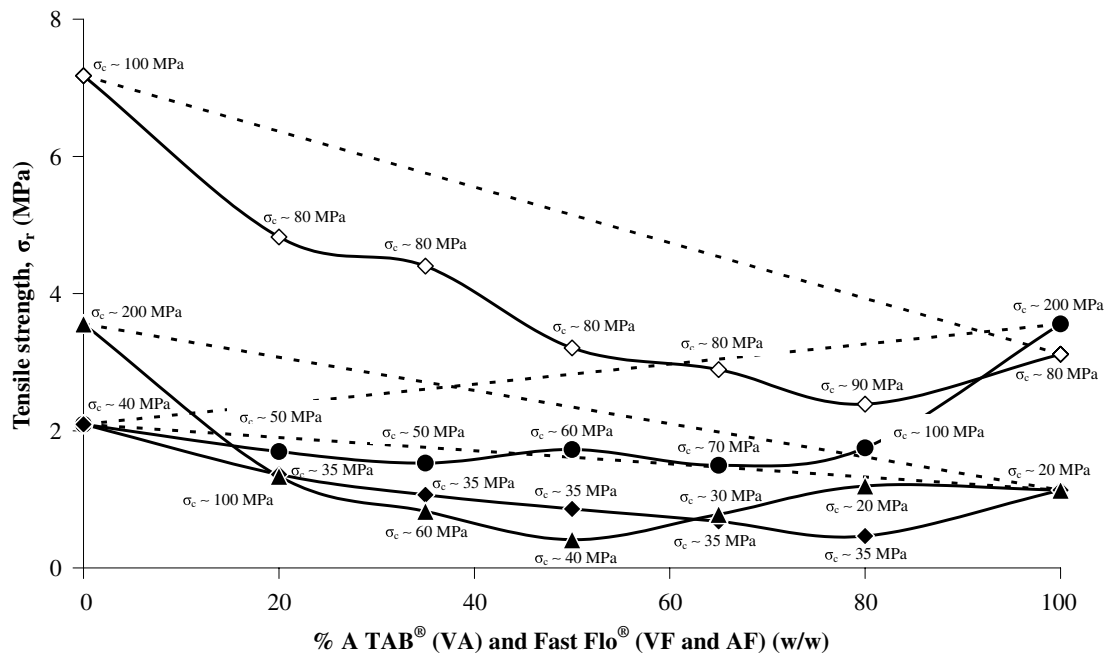


Fig. 6. Tensile strength (σ_t , interpolated values) as a function of binary mixture composition (w/w) for compact mean porosities (ε). The dotted line represents the result of the use of a linear simple mixing rule. σ_c is the compaction pressure applied to obtain the corresponding σ_t values. Key: ●, VA (with $\varepsilon = 35\%$); ◇ and ◆, VF (with $\varepsilon = 20\%$ and 35%); ▲, AF (with $\varepsilon = 20\%$).

seems to decrease linearly, with a slope approximately equal to the linear rule.

VA mixtures (circle symbols in Fig. 6). In the whole range of mixture compositions, values smaller than the tensile strength of both single materials are observed. At small A proportions, the tensile strength slightly decreases and becomes a bit smaller than the σ_r value of V. Between 20% and 70% of A, the lowest values are obtained. Then, the tensile strength increases abruptly above 80% w/w to reach the A value. When the proportions of A are high enough, it is thought that the percolating network of V particles disappears (mass proportions higher than 70%). This leads to an increase of the tensile strength.

AF mixtures (triangular symbols in Fig. 6). These mixtures show an important decrease in compact tensile strength with increasing F proportions. The minimum which is observed occurs for a F around 50% in mass, and is well below the one of the two single materials. The tensile strength increases again and reaches the one of F at 80% w/w about. Above this concentration, it seems to remain constant.

3.2.3. Brinell hardness

The variations of the Brinell hardness of compacts are observed as a function of the mixture composition (Fig. 7) for a constant mean porosity of $\varepsilon = 35\%$ (and also at $\varepsilon = 20\%$ in the case of VF mixtures). Like for the two other mechanical properties (E and σ_r), the variations of the Brinell hardness with the mixture composition cannot be described by a simple linear mixing rule, and a negative deviation from this rule is observed.

VA and VF mixtures (circle and diamond-shaped symbols, respectively, in Fig. 7). The Brinell hardness shows a rather constant value for concentrations below 75% w/w of F and A, which corresponds to the Brinell hardness of V. This could be explained by the fact that V undergoes plastic deformation at small applied pressure ($P_y = 54$ MPa [16,17]) and spreads on the surface of the compact. Leuenberger et al. [31] observed the same tendency of the Brinell hardness with cylindrical tablets of mixtures of sodium lauryl sulfate/cafeine (which are also plastic/brittle mixtures). The Brinell hardness starts to increase when the V proportions are no longer enough to cover all the compact surface. For these mixtures, this happens for A and F proportions above around 75% in mass. In the special case of the VA mixtures, this correlates with the results of Holman and Leuenberger [32] which observed very little variations of the Brinell hardness of microcrystalline cellulose/dihydrate calcium phosphate mixtures for volume fraction of the calcium phosphate phase smaller than 69% (this proportion corresponds to a mass concentration of 77%).

AF mixtures (triangular symbols in Fig. 7). The Brinell hardness increases continuously from F to A; but the evolution is divided in two linear zones which intercept for a critical concentration of F around 25% w/w. For A proportions lower than 65% w/w, the Brinell hardness changes much less than for large proportions of A (>65% w/w). This could be due to the fact that F is more plastic ($P_y = 111$ MPa) than A ($P_y = 530$ MPa).

One shall then conclude that at least one of the two percolation thresholds cannot be detected from the variations

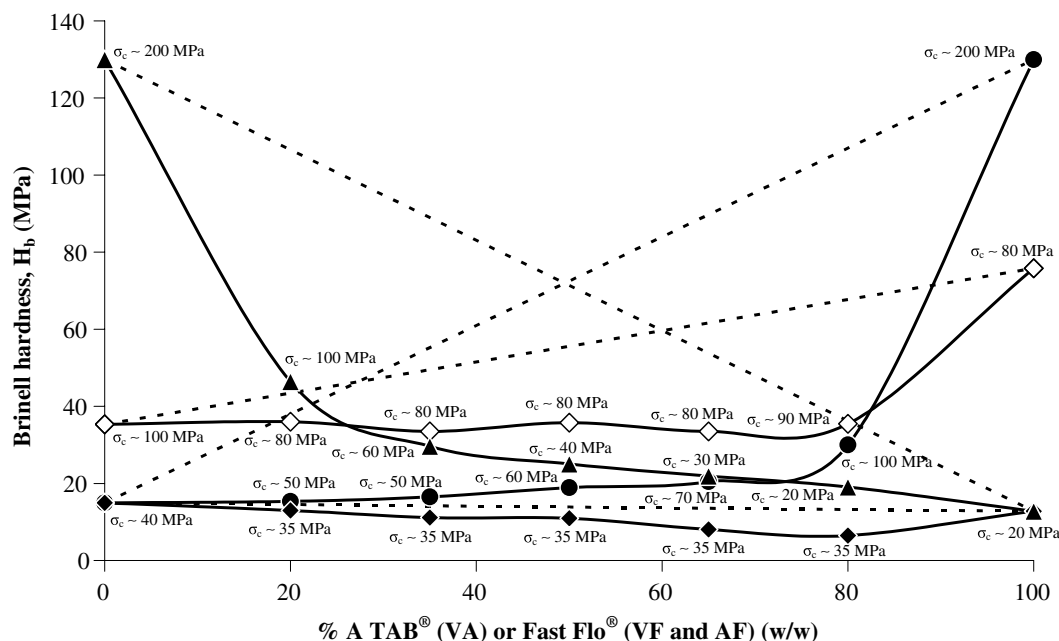


Fig. 7. Brinell hardness (H_b , interpolated values) as a function of binary mixture composition (w/w) for compact mean porosities (ε). The dotted line represents the result of the use of a linear simple mixing rule. σ_c is the compaction pressure applied to obtain the corresponding H_b values. Key: ●, VA (with $\varepsilon = 35\%$); ◇ and ◆, VF (with $\varepsilon = 20\%$ and 35%); ▲, AF (with $\varepsilon = 35\%$).

of the Brinell hardness, whatever the mixture presently studied. On the other hand, one of the percolation thresholds may correspond to the turn of variations observed. However, this turn occurs always around 80% in mass whatever the density ratio of the two mixed compounds (see Table 1), that indicates a not constant volume ratio at turn, so that the turn does not correspond to a fix ratio of volume hence to a fix percolation threshold.

3.3. Proposal of a model for the mechanical properties of binary mixtures

The previous experimental results have shown that it was not possible to describe the variation of the mechanical properties of binary mixtures using a simple linear mixing rule. In order to describe the negative deviation observed with all the mixtures, a statistical model based on a classic thermodynamic approach was proposed [31,33,34]. It allows one to obtain interaction parameters which characterize the affinity of the two compounds to each other. This model was applied to the Young's modulus and the tensile strength.

3.3.1. Statistical model, 1st approach, i.e. binary interactions

A binary mixture AB with a proportion x of A is considered. In this mixture, there are three possible binary interactions, A–A, B–B and A–B (B–A). According to a statistical approach [33,34], the fraction x of the component A and $(1 - x)$ of the component B in the system represent their distribution probability. Then, the probability of having two A particles as a neighbour is x^2 , and for each interaction, it is possible to calculate the statistical weight (Table 4).

Using this statistical approach, a property Y of a mixture AB can be expressed by the following relationship:

$$Y = x^2 \cdot Y_{AA} + (1 - x)^2 \cdot Y_{BB} + 2x \cdot (1 - x) \cdot Y_{AB}, \quad (8)$$

where Y_{AA} and Y_{BB} are the properties of the single materials (corresponding to the A–A and B–B interactions) and Y_{AB} is the property resulting from the A–B and B–A interactions which are supposed to be identical.

Eq. (8) can be developed to obtain Eq. (9)

$$Y = x \cdot Y_{AA} + (1 - x) \cdot Y_{BB} + x \cdot (1 - x) \cdot [2Y_{AB} - Y_{AA} - Y_{BB}] \quad (9)$$

So, labelling

$$Y_{ww} = 2Y_{AB} - Y_{AA} - Y_{BB} \quad (10)$$

Eq. (9) transforms into Eq. (11)

$$Y = x \cdot Y_{AA} + (1 - x) \cdot Y_{BB} + x \cdot (1 - x) \cdot Y_{ww}, \quad (11)$$

where Y_{ww} is the interaction term for the Y property.

When $Y_{ww} = 0$, Eq. (11) corresponds to a simple linear mixing rule (shown by the dotted line in Figs. 5 and 6)

$$Y = x \cdot Y_{AA} + (1 - x) \cdot Y_{BB}. \quad (12)$$

When $Y_{ww} < 0$, a negative deviation from the linear mixing rule is observed. On the contrary, when $Y_{ww} > 0$, the deviation is positive.

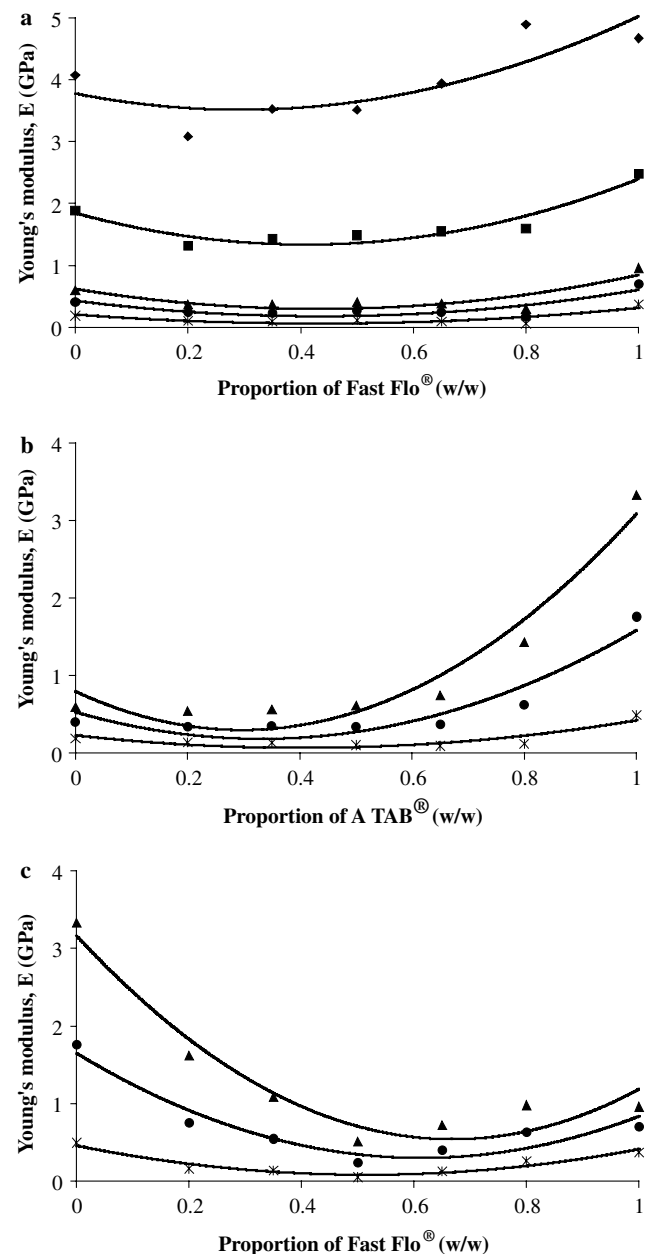


Fig. 8. Young's modulus (E , interpolated values) of binary mixture vs. the mixture composition for a constant compact mean porosity (ϵ). The 1st approach of the proposed model is used (full line). (a) Vivapur 12[®]/Fast Flo[®] mixtures; (b) Vivapur 12[®]/A TAB[®] mixtures; (c) A TAB[®]/Fast Flo[®] mixtures. Key: ♦, $\epsilon = 10\%$; ■, $\epsilon = 20\%$; ▲, $\epsilon = 35\%$; ●, $\epsilon = 40\%$; *, $\epsilon = 50\%$.

Table 4

Statistical weights attributed to the different possible interactions in the 1st approach of the proposed model

Interactions	A–A	B–B	A–B	B–A
Statistical weights	x^2	$(1 - x)^2$	$x(1 - x)$	$(1 - x)x$

3.3.2. Use of the 1st approach for the Young's modulus and the tensile strength of binary mixtures

The variations of the Young's modulus and the tensile strength for various compact porosities are given in Figs. 8 and 9. The E and σ_r values vs. the mass fractions of the two components are fitted with a quadratic equation (full lines in Figs. 8 and 9). It appears that the E and σ_r values seem to be relatively well represented by a quadratic equation (see correlation coefficients R^2 in Table 5). Nevertheless, the critical mass fractions do not appear with this approach. The constant value observed with the Young's

Table 5

R^2 values obtained for the binary mixtures using the 1st and the 2nd approach of the proposed model

Mixtures	ε (%)	1st approach		2nd approach	
		R^2 (E)	R^2 (σ_r)	R^2 (E)	R^2 (σ_r)
VF	10	0.6839	0.9506	0.9057	0.9566
	20	0.8948	0.9790	0.8980	0.9797
	35	0.7418	0.9444	0.8297	0.9645
	40	0.7263	0.9256	0.8309	0.9551
	50	0.7185	0.8889	0.8428	0.9376
VA	35	0.9429	0.8467	0.9973	0.9449
	40	0.8972	0.7818	0.9909	0.8651
	50	0.7903	0.4930	0.9644	0.6956
AF	35	0.9434	0.8755	0.9869	0.9905
	40	0.9173	0.8564	0.9796	0.9793
	50	0.9152	0.9198	0.9681	0.9616

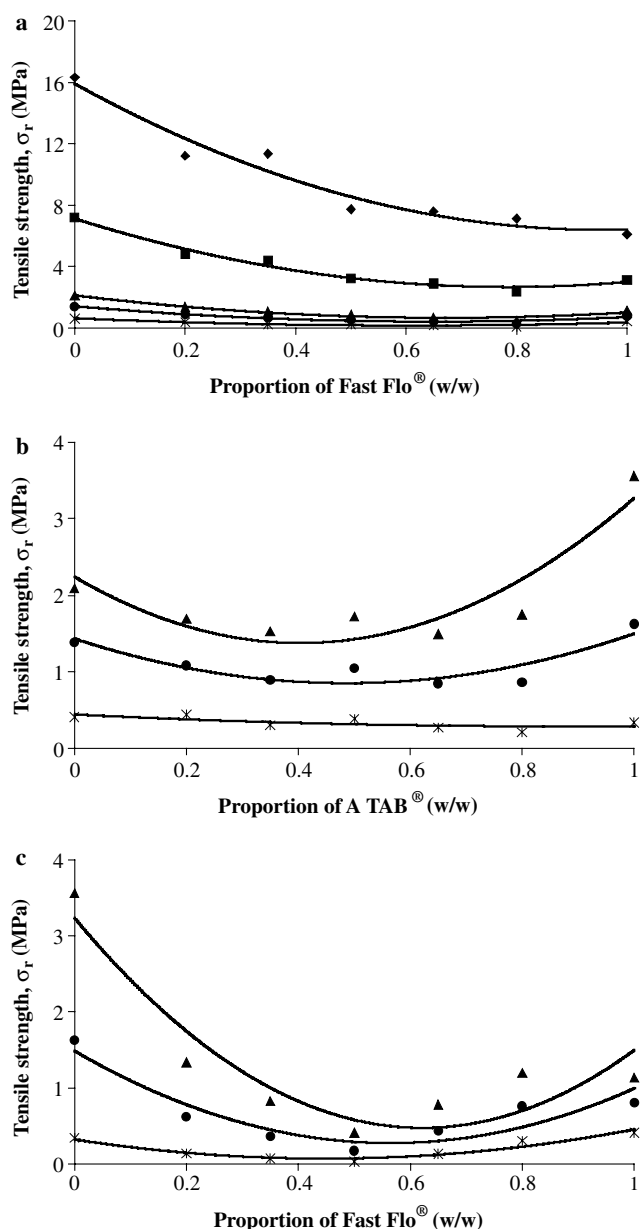


Fig. 9. Tensile strength (σ_r , interpolated values) of binary mixture vs. the mixture composition for a constant compact mean porosity (ε). The 1st approach of the proposed model is used (full line). (a) Vivapur 12[®]/Fast Flo[®] mixtures; (b) Vivapur 12[®]/A TAB[®] mixtures; (c) A TAB[®]/Fast Flo[®] mixtures. Key: \blacklozenge , $\varepsilon = 10\%$; \blacksquare , $\varepsilon = 20\%$; \blacktriangle , $\varepsilon = 35\%$; \bullet , $\varepsilon = 40\%$; $*$, $\varepsilon = 50\%$.

modulus of the VA and the AF mixtures and the minimum value observed with the tensile strength of the same mixtures are not well described. More, the parameters corresponding to E or σ_r of the single materials slightly differ between different binary mixtures (see Table 6).

The parameters used in Eq. (11) for the best fits are displayed in Table 6. In all the cases, the interaction parameters E_{ww} and σ_{rww} are negative. This is in accordance with the fact that a negative deviation from a linear mixing rule is experimentally observed. The values of the interaction parameters could be linked to the affinity of the mixture components [31]. Negative interaction parameters mean that the interactions between same components are stronger than between different materials (i.e. that the cohesive forces are more important). For porosities between 35% and 50%, the absolute values of the interaction parameters which are obtained in VA mixtures are larger than for VF mixtures. This means that V particles have more affinity for F than for A. On the other hand, the closed values of the parameters in the case of AF and VA mixtures show that the affinities of A for F and V are of the same order.

3.3.3. Statistical model, 2nd approach, i.e. triplet interactions

In a second step, the model was improved to take into account the environment of the interactions. In the second version of the model, binary interactions were replaced by triplet interactions (Table 7). This approach takes into account the surroundings of each link. More, a triangular interaction is supposed to be more rigid than binary interaction. It was expected that this version could describe with more accuracy the hardness and the strength of the compacted system.

Similar to the 1st approach, the fraction x of the component A and $(1 - x)$ of the component B are introduced in the model and used to link each triplet term {AAA, AAB, ABB, BBB} with their corresponding statistical weight $\{x^3, 3x^2 \cdot (1 - x), 3x \cdot (1 - x)^2, (1 - x)^3\}$ (Table 7). Each

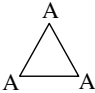
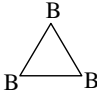
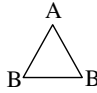
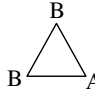
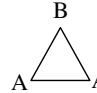
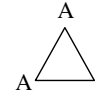
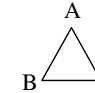
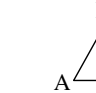
Table 6

Calculated parameters obtained using a quadratic equation for the Young's modulus and the tensile strength (E_{FF} , E_{VV} , E_{AA} , E_{ww} : GPa; σ_{rFF} , σ_{rVV} , σ_{rAA} , σ_{rww} : MPa)

Mixtures	ε (%)	Model parameters, E			Model parameters, σ_r		
		E_{FF}	E_{VV}	E_{ww}	σ_{rFF}	σ_{rVV}	σ_{rww}
VF	10	5.03	3.78	−3.03	6.41	15.91	−10.45
	20	2.40	1.85	−3.04	3.00	7.12	−7.23
	35	0.84	0.62	−1.71	1.01	2.12	−3.23
	40	0.60	0.43	−1.34	0.71	1.42	−2.39
	50	0.31	0.21	−0.78	0.35	0.63	−1.27
VA		E_{AA}	E_{VV}	E_{ww}	σ_{rAA}	σ_{rVV}	σ_{rww}
	35	3.09	0.79	−5.64	3.27	2.24	−5.31
	40	1.58	0.53	−3.13	1.50	1.43	−2.45
	50	0.42	0.23	−0.99	0.29	0.45	−0.21
AF		E_{FF}	E_{AA}	E_{ww}	σ_{rFF}	σ_{rAA}	σ_{rww}
	35	1.18	3.16	−5.87	1.50	3.23	−7.14
	40	0.83	1.65	−3.59	0.99	1.49	−3.80
	50	0.41	0.46	−1.41	0.45	0.32	−1.26

Table 7

Statistical weights attributed to the different possible interactions in the 2nd approach of the proposed model

Interactions								
Statistical weights	x^3	$(1-x)^3$	$x(1-x)^2$	$(1-x)^2x$	$(1-x)x^2$	$x^2(1-x)$	$x^2(1-x)$	$(1-x)x(1-x)$

weight is then modulated by an interaction term whose strength depends on the nature of the property Y . So, with reference to the Eq. (8), a property Y of the system is expressed by the following equation:

$$Y = x^3 \cdot Y_{AAA} + (1-x)^3 \cdot Y_{BBB} + 3x \cdot (1-x)^2 \cdot Y_{ABB} + 3x^2 \cdot (1-x) \cdot Y_{BAA} \quad (13)$$

Using $x = 0$ and $x = 1$ shows that Y_{AAA} and Y_{BBB} are the properties of the single materials. Y_{ABB} and Y_{BAA} are the properties of the {AAB} and {BAA} interactions. Eq. (13) is rearranged:

$$Y = x \cdot Y_{AAA} + (1-x) \cdot Y_{BBB} + x^2 \cdot (1-x) \cdot [3Y_{BAA} - 2Y_{AAA} - Y_{BBB}] + x \cdot (1-x)^2 \cdot [3Y_{ABB} - Y_{AAA} - 2Y_{BBB}] \quad (14)$$

If the two interaction terms Y_{ww1} and Y_{ww2} are expressed by the two following equations:

$$Y_{ww1} = 3Y_{BAA} - 2Y_{AAA} - Y_{BBB}, \quad (15)$$

$$Y_{ww2} = 3Y_{ABB} - Y_{AAA} - 2Y_{BBB}. \quad (16)$$

Eq. (14) can be written as:

$$Y = x \cdot Y_{AAA} + (1-x) \cdot Y_{BBB} + x^2 \cdot (1-x) \cdot Y_{ww1} + x \cdot (1-x)^2 \cdot Y_{ww2} \quad (17)$$

When $Y_{ww1} = 0$ and $Y_{ww2} = 0$, a simple linear mixing rule is observed. When the two interaction parameters are negative, a negative deviation from the linear mixing rule is obtained. On the contrary, when these parameters have a positive value, the deviation is positive.

3.3.4. Use of the 2nd approach for the Young's modulus and the tensile strength of binary mixtures

The use of the 2nd approach for the Young's modulus and the tensile strength of the studied binary mixtures is shown in Figs. 10 and 11. The E and σ_r values vs. the mass fractions of the two components are fitted with a cubic equation (full lines in Figs. 10 and 11). This second approach using a cubic equation seems to describe more accurately the change of the two mechanical properties with the mixture composition. This is represented by better R^2 values than in the case of the 1st approach (Table 5). Contrary to the 1st approach, the critical mass fractions could be visualized and the coefficients for the mechanical properties of the single materials are in the same order whatever the mixture composition may be. For example, E_{FFF} obtained with VF mixtures at a porosity of 35% is 0.91 GPa and E_{FFF} obtained with AF mixtures is 0.99 GPa at the same porosity. The same trend is observed with the two other excipients (see Table 8). Then, it may be predictive from the properties of individual components.

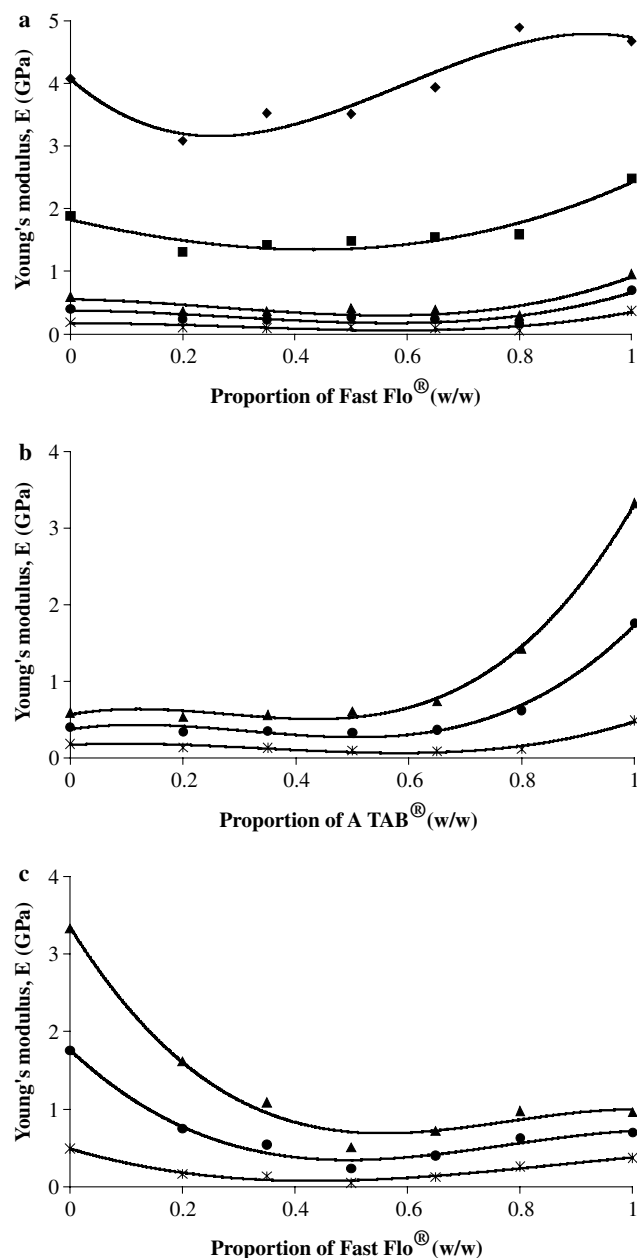


Fig. 10. Young's modulus (E , interpolated values) of binary mixture vs. the mixture composition for a constant compact mean porosity (ε). The 2nd approach of the proposed model is used (full line). (a) Vivapur 12[®]/Fast Flo[®] mixtures; (b) Vivapur 12[®]/A TAB[®] mixtures; (c) A TAB[®]/Fast Flo[®] mixtures. Key: \blacklozenge , $\varepsilon = 10\%$; \blacksquare , $\varepsilon = 20\%$; \blacktriangle , $\varepsilon = 35\%$; \bullet , $\varepsilon = 40\%$; $*$, $\varepsilon = 50\%$.

The parameters of Eq. (17) are calculated by a best fit procedure and reported in Table 8. Similarly to the 1st approach, the interaction parameters E_{ww1} , E_{ww2} and σ_{rww1} , σ_{rww2} are negative (except E_{ww1} of VF mixture with $\varepsilon = 10\%$, E_{ww2} of VA mixture with $\varepsilon = 50\%$ and σ_{rww2} of VA mixture with $\varepsilon = 50\%$). These values correspond to the negative deviation from a linear mixing rule which is experimentally observed. The interaction parameters which correspond to a majority of A (i.e., interactions {VAA} and {FAA}) show the most important

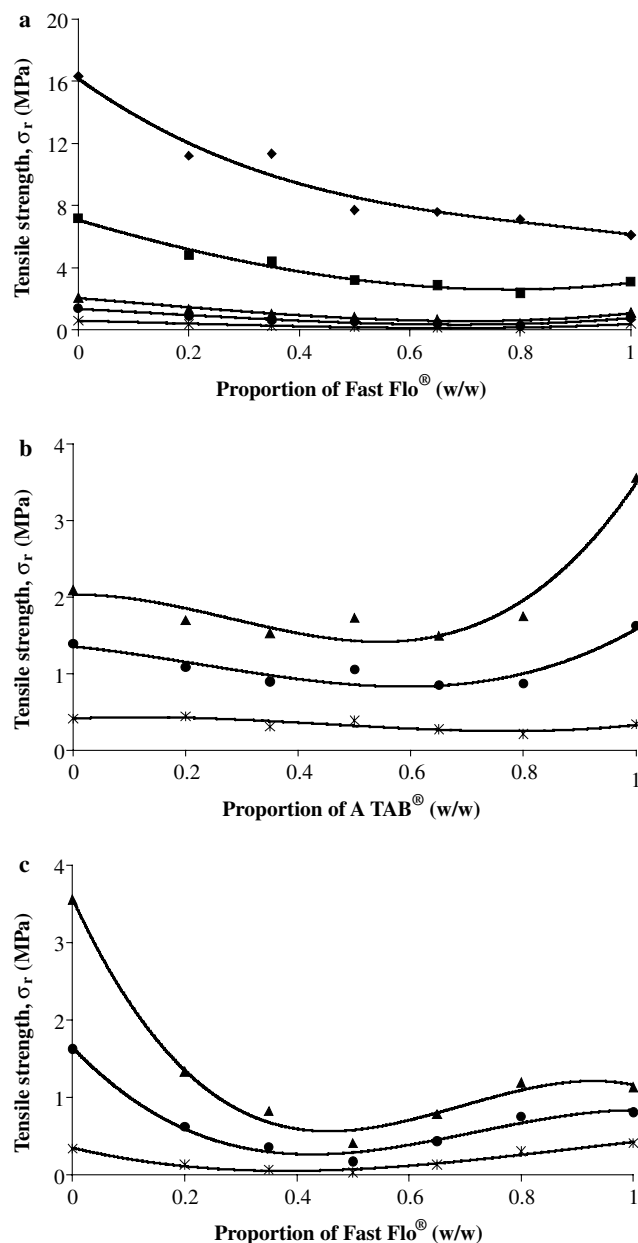


Fig. 11. Tensile strength (σ_r , interpolated values) of binary mixture vs. the mixture composition for a constant compact mean porosity (ε). The 2nd approach of the proposed model is used (full line). (a) Vivapur 12[®]/Fast Flo[®] mixtures; (b) Vivapur 12[®]/A TAB[®] mixtures; (c) A TAB[®]/Fast Flo[®] mixtures. Key: \blacklozenge , $\varepsilon = 10\%$; \blacksquare , $\varepsilon = 20\%$; \blacktriangle , $\varepsilon = 35\%$; \bullet , $\varepsilon = 40\%$; $*$, $\varepsilon = 50\%$.

absolute values (E_{ww1} and σ_{rww1} of VA mixture and E_{ww2} and σ_{rww2} of AF mixture). This means that V and F have a low affinity for A, but a high affinity between them. More, these interaction parameters have values which are in the same order for porosities between 35% and 50%. These values mean that the affinity of A for F and V is in the same order. Similar to the 1st approach, the interaction parameters point out that the affinity of V for F is more important than the affinity for A.

Table 8

Calculated parameters obtained using a cubic equation for the Young's modulus and the tensile strength (E_{FFF} , E_{VVV} , E_{AAA} , E_{ww1} , E_{ww2} : GPa; σ_{rFFF} , σ_{rVVV} , σ_{rAAA} , σ_{rww1} , σ_{rww2} : MPa)

Mixtures	ε (%)	Model parameters, E				Model parameters, σ_r			
		E_{FFF}	E_{VVV}	$E_{\text{ww1}}(\text{VFF})$	$E_{\text{ww2}}(\text{FVV})$	σ_{rFFF}	σ_{rVVV}	$\sigma_{\text{rww1}}(\text{VFF})$	$\sigma_{\text{rww2}}(\text{FVV})$
VF	10	4.73	4.07	2.38	−8.44	6.15	16.17	−5.58	−15.33
	20	2.42	1.82	−3.44	−2.64	3.04	7.08	−8.02	−6.44
	35	0.91	0.55	−2.91	−0.51	1.08	2.05	−4.56	−1.90
	40	0.66	0.37	−2.37	−0.31	0.77	1.36	−3.50	−1.28
	50	0.35	0.17	−1.44	−0.12	0.39	0.60	−1.96	−0.59
VA		E_{AAA}	E_{VVV}	$E_{\text{ww1}}(\text{VAA})$	$E_{\text{ww2}}(\text{AVV})$	σ_{rAAA}	σ_{rVVV}	$\sigma_{\text{rww1}}(\text{VAA})$	$\sigma_{\text{rww2}}(\text{AVV})$
	35	3.31	0.57	−9.85	−1.43	3.48	2.03	−9.30	−1.32
	40	1.73	0.38	−5.93	−0.33	1.58	1.35	−3.94	−0.95
	50	0.48	0.17	−2.02	0.04	0.33	0.41	−0.85	0.44
		E_{FFF}	E_{AAA}	$E_{\text{ww1}}(\text{AFF})$	$E_{\text{ww2}}(\text{FAA})$	σ_{rFFF}	σ_{rAAA}	$\sigma_{\text{rww1}}(\text{AFF})$	$\sigma_{\text{rww2}}(\text{FAA})$
AF	35	0.99	3.35	−2.37	−9.37	1.16	3.57	−0.97	−13.32
	40	0.72	1.76	−1.42	−5.76	0.84	1.64	−0.88	−6.71
	50	0.38	0.49	−0.77	−2.04	0.42	0.35	−0.73	−1.79

Then, this 2nd approach is predictive for the properties of the three single materials studied using the tests performed on binary mixtures. Nevertheless, knowing E and σ_r of the single compounds, it is not possible to have a straight prediction of E and σ_r for a binary mixture. It is necessary to perform at least one test to obtain the interaction parameter.

3.4. X-ray tomography of the binary mixtures

According to the Beer–Lambert law (see Eq. (7)), the attenuation of the X-ray beam depends on the density of the tested material. For binary mixtures, the two components can be detected if the two apparent particular densities are differentiated and if the pixel resolution of the

cross-section is smaller than the particle sizes. So, in our systems, these two last conditions are verified and, the X-ray tomography technique can be used for the binary mixtures with A. Here, only VA mixtures compacted under 120 MPa were studied. Fig. 12 shows the horizontal (x – y) cross-section at mid-height of the sample obtained for the various compositions of the VA mixtures. In this figure, V is blue and A red. Contrary to previous studies performed on compacts of single components [16,29,35], it is not possible to detect the heterogeneity in density resulting from compaction, since this heterogeneity is less important than the variation between the apparent particular densities of V and A. But, it appears that V is preferentially localized near the sample surfaces from a V mass proportion of 20%. In Fig. 12, the applied compaction pressure

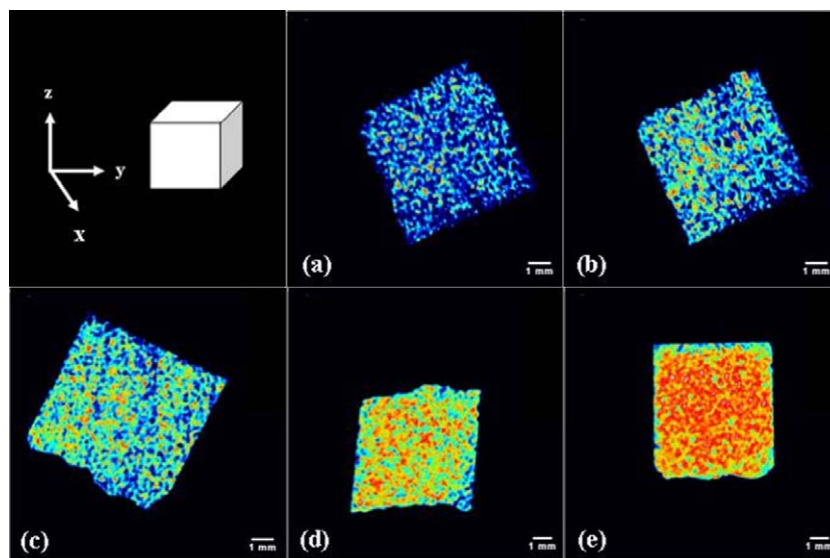


Fig. 12. Horizontal (x – y) cross-sections at mid-height of the compacted samples for the VA mixtures compacted under 120 MPa. (a) VA82, (b) VA63, (c) VA55, (d) VA36, (e) VA28.

(120 MPa) exceeds the mean yield pressure of V ($P_y = 54$ MPa) [17]. Then, for this compaction pressure, V deforms plastically and spreads especially near the die walls. Leuenberger and Rohera [31] observed the same behaviour with a binary mixture of brittle/plastic materials on SEM photographs. This observation could explain that the Brinell hardness of the VA mixtures compacted at 120 MPa is about those of V compacts for A concentrations between 0% and 80% w/w (see Fig. 13). Then, due to the “skin” of the most plastic material in the compacts’ surface, the hardness of the compacted mixtures using a microindentation test cannot be obtained. The measurement corresponds to the hardness of the material that is in surface. This correlates with the values of Brinell hardness obtained with compacted mixtures that are measured on compacts of the material with the lowest P_y (see Section 3.2.3). More, except the compact surfaces, the mixture seems homogeneous, no segregation effects are visible at this length scale (superior to 15 μm). According to percolation theory [12] and keeping in mind that Fig. 12 shows 2D cross-sections, it is possible to observe the two critical mass compositions of V and A for about 35% and 65% w/w of A. These two concentrations correspond to the fractions

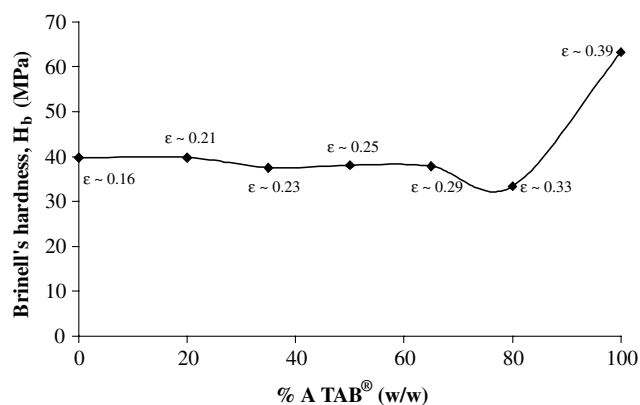


Fig. 13. Variation of the Brinell hardness (H_b) of VA mixtures vs. the mixture composition for a compaction pressure of 120 MPa. ϵ is the mean porosity of the sample compacted at 120 MPa.

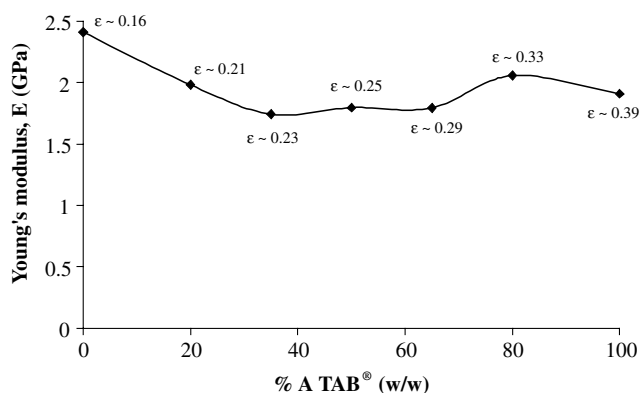


Fig. 14. Variation of the Young's modulus (E) of VA mixtures vs. the mixture composition for a compaction pressure of 120 MPa. ϵ is the mean porosity of the sample compacted at 120 MPa.

when A (35% w/w of A) and V (65% w/w of A) begin to form a percolating particle network. Between these two proportions (case of the VA55 mixture in Fig. 12), the two materials coexist as two percolating networks. These values are in good accordance with those obtained from the variation of the Young's modulus with the mixture composition for samples obtained under 120 MPa (Fig. 14).

4. Conclusion

Three mechanical properties of tablets made of single component (Vivapur 12®, Fast Flo® and A TAB®) and of their binary mixtures (with various mass concentrations) were studied. It was shown that the mechanical properties compared at a constant porosity are not a linear function of the mass concentration of the two components in the binary mixture. More, a negative deviation from a proportional relationship was always observed. In accordance with the composition percolation theory, critical mass fractions were detected. In the special case of the Brinell hardness which is a property of the compact surface, it was observed that the most plastic material of the two controls the mixture behaviour from little concentrations in the mixture. Since a simple linear mixing rule did not hold, a predictive model based on a classic thermodynamic approach was proposed. Two approaches based on the type of components interactions were used. The validity of the model was demonstrated on experimental data for the studied binary mixtures. In the case of the Young's modulus and the tensile strength, it seemed that the second approach, based on triplet interactions between the two components of the mixture, was more adapted. More, an interaction parameter which characterizes the mutual affinity of the two components was obtained. Finally, the X-ray tomography technique was applied to one of the binary mixtures (cellulose/phosphate mixtures) compacted under 120 MPa. Images analysis showed that the compacts were not heterogeneous in density. Indeed, Vivapur 12® was preferentially observed in the periphery of the compact (i.e. near the surface). This confirmed the previous results obtained with the Brinell hardness. It was also possible to detect visually the critical mass concentrations of the two excipients.

References

- [1] M. Sheikh-Salem, J.T. Fell, Compaction characteristics of mixtures of materials with dissimilar compaction mechanisms, *Int. J. Pharm. Tech. Prod. Mfr.* 2 (1981) 19–22.
- [2] P. Humber-Droz, D. Mordier, E. Doelker, Densification behaviour of powder mixtures, *Acta Pharm. Technol.* 29 (1983) 69–73.
- [3] B. Van Veen, K. Van der Voort Maarschalk, G.K. Bolhuis, K. Zuurman, H.W. Frijlink, Tensile strength of tablets containing two materials with a different compaction behaviour, *Int. J. Pharm.* 203 (2000) 71–79.
- [4] J. Zheng, W.B. Carlson, J.S. Reed, The packing density of binary powder mixtures, *J. Eur. Ceram. Soc.* 15 (1995) 479–483.

- [5] C.M. Ramaswamy, Y.B.G. Varma, D. Venkateswarlu, Compaction of mixtures of materials, *Chem. Eng. J.* 1 (1970) 168–171.
- [6] W. Jetzer, Compaction characteristics of binary mixtures, *Int. J. Pharm.* 31 (1986) 201–207.
- [7] J. Ilkka, P. Paronen, Prediction of the compression behaviour of powder mixtures by the Heckel equation, *Int. J. Pharm.* 94 (1993) 181–187.
- [8] J.T. Fell, Compaction properties of binary mixtures; pharmaceutical powder compaction technology, *Drugs and the pharmaceutical Sciences*, 71, 1996, pp. 501–515.
- [9] H. Leuenberger, Compression of binary powder mixtures and solubility parameters of solids, *Int. J. Pharm.* 27 (1985) 127–138.
- [10] B. Van Veen, K. Maarschalk, G.K. Bolhuis, H.W. Frijlink, Predicting mechanical properties of compacts containing two components, *Powder Technol.* 139 (2004) 156–164.
- [11] H. Leuenberger, The application of percolation theory in powder technology, *Adv. Powder Technol.* 10 (1999) 323–352.
- [12] D. Bouvard, Densification behaviour of mixtures of hard and soft powders under pressure, *Powder Technol.* 111 (2000) 231–239.
- [13] D. Blattner, M. Kolb, H. Leuenberger, Percolation theory and compactibility of binary powder systems, *Pharm. Res.* 7 (1990) 113–117.
- [14] L.E. Holman, The compaction behaviour of particulate materials. An elucidation based on percolation theory, *Powder Technol.* 66 (1991) 265–280.
- [15] H. Leuenberger, The compressibility and compactibility of powder systems, *Int. J. Pharm.* 12 (1982) 41–55.
- [16] V. Busignies, Recherche de lois de mélange sur des propriétés mécaniques de systèmes granulaires compactés, PhD Thesis, University of Paris 11, France, 2005.
- [17] V. Busignies, B. Leclerc, G. Couarraze, P. Tchoreloff, Compaction behaviour and new predictive approach to the compressibility of binary mixtures of pharmaceutical excipients, *Eur. J. Pharm. Biopharm.*, in press, 2006.
- [18] W. Heckel, An analysis of powder compaction phenomena, *Trans. Metal. Soc. A.I.M.E.* 221 (1961) 671–675.
- [19] W. Heckel, Density–pressure relationship in powder compaction, *Trans. Metal. Soc. A.I.M.E.* 221 (1961) 1001–1008.
- [20] C.-Y. Wu, S.M. Best, A.C. Bentham, B.C. Hancock, W. Bonfird, A simple predictive model for the tensile strength of binary tablets, *Eur. J. Pharm. Sc.* 25 (2005) 331–336.
- [21] V. Busignies, P. Tchoreloff, B. Leclerc, M. Besnard, G. Couarraze, Compaction of crystallographic forms of pharmaceutical granular lactoses. I. Compressibility, *Eur. J. Pharm. Biopharm.* 58 (2004) 569–576.
- [22] D. Bielawski, G. Couarraze, B. Leclerc, P. Tchoreloff, Procédé et micropresse pour caractériser les propriétés mécaniques des solides pharmaceutiques: World Patent WO 02084254, 2002.
- [23] V. Busignies, P. Tchoreloff, B. Leclerc, C. Hersen, G. Keller, G. Couarraze, Compaction of crystallographic forms of pharmaceutical granular lactoses. II. Compacts mechanical properties, *Eur. J. Pharm. Biopharm.* 58 (2004) 577–586.
- [24] H. Leuenberger, B.D. Rohera, Fundamentals of powder compression. I. The compactibility and compressibility of pharmaceutical powders, *Pharm. Res.* 3 (1986) 12–21.
- [25] E. Ryshkewitch, Compression strength of porous sintered alumina and zirconia, *J. Am. Ceram. Soc.* 36 (1953) 65–68.
- [26] J.M. Spriggs, Expression for effect of porosity on elastic modulus of polycrystalline refractory materials, particularly aluminum oxide, *J. Am. Ceram. Soc.* 44 (1961) 628–629.
- [27] A.C. Kak, Computerized tomography with X-ray, emission and ultrasound sources, *Proc. IEEE* 9 (1979) 1245–1272.
- [28] D.H. Phillips, J.J. Lannutti, Measuring physical density with X-ray computed tomography, *NDT&E Int.* 30 (1997) 339–350.
- [29] I.C. Sinka, S.F. Burch, J.H. Tweed, J.C. Cunningham, Measurement of density variations in tablets using X-ray computed tomography, *Int. J. Pharm.* 271 (2004) 215–224.
- [30] W. S. Rasband, ImageJ 1.32j. National Institutes of Health, Bethesda, Maryland, USA, 1997–2005. <<http://rsb.info.nih.gov/ij/>>.
- [31] H. Leuenberger, B.D. Rohera, Fundamentals of powder compression. II. The compression of binary powder mixtures, *Pharm. Res.* 3 (1986) 65–74.
- [32] L.E. Holman, H. Leuenberger, The effect of varying the composition of binary powder mixtures and compacts on their properties: a percolation phenomenon, *Powder Technol.* 60 (1990) 249–258.
- [33] P. Papon, J. Leblond, *Thermodynamique des fluides; Thermodynamique des états de la matière*, 1990, pp. 283–285.
- [34] P. Papon, J. Leblond, *Propriétés thermodynamiques de l'état solide; Thermodynamique des états de la matière*, 1990, pp. 327–330.
- [35] V. Busignies, B. Leclerc, P. Porion, P. Evesque, G. Couarraze, P. Tchoreloff, Quantitative measurements of localized density variations in cylindrical tablets using X-ray microtomography, *Eur. J. Pharm. Biopharm.*, in press, 2006.